Journal of Alloys and Compounds 509 (2011) 5789–5795

Contents lists available at ScienceDirect

Journal of Alloys and Compounds

journal homepage: www.elsevier.com/locate/jallcom

Study on the structure and surface acoustic wave properties of SNGS and STGS piezoelectric crystals

Beibei Qiu[a], Guiwu Lu[a,*], Yuqiu Jiao[a], Chong Wu[a], Guanggang Zhou[a], Chao Feng[a], Wenqi Huang[b], Hong Yang[b]

[a] State key laboratory of heavy oil processing, College of science, China University of Petroleum, Beijing 102249, People's Republic of China
[b] College of science Beijing information science & technology university, Beijing 100192, People's Republic of China

ARTICLE INFO

Article history:
Received 12 October 2010
Received in revised form 21 February 2011
Accepted 22 February 2011
Available online 1 March 2011

Keywords:
SNGS
STGS
The first principles
The phase velocity
Electromechanical coupling factor
PFA

ABSTRACT

The geometry structure, band structure and density of states of $Sr_3NbGa_3Si_2O_{14}$ (SNGS) and $Sr_3TaGa_3Si_2O_{14}$ (STGS) single crystals were investigated by using density functional theory (DFT) method. Parameters including the phase velocity, electromechanical coupling factor and power flow angle (PFA) were calculated for SNGS and STGS at X, Y, Z cuts, respectively. Our calculated data are in good agreement with the experimental results. It is found that the peaks of partial density of states of Sr, Ga, Si and O atoms of STGS have a tendency of shifting to the higher energy levels relative to those of SNGS. Compared with quartz, SNGS and STGS crystals are of lower phase velocities and higher electromechanical coupling factor. The propagation direction of 167.5° of X-cut SNGS, 0° of Y-cut SNGS and 170° of X-cut STGS are found to be optimum direction for SAW device applications.

1. Introduction

Langasite structure compounds have been the focus of much consideration recently as promising new materials for acoustic device applications. Langasite-type crystals such as $La_3Ga_5SiO_{14}$ (LGS) [1], $La_3Ga_{5.5}Nb_{0.5}O_{14}$ (LGN) [2], $La_3Ga_{5.5}Ta_{0.5}O_{14}$ (LGT) [3] are good piezoelectric materials. Compared with quartz, langasite-type crystals have higher electromechanical coupling coefficient and lower acoustic velocities. They can be applied to fabricate miniaturized intermediate frequency band-pass filters which have been used widely in the radar, communication and navigation system. Due to the excellent behavior with high electromechanical coupling coefficient and low acoustic velocities up to their melting points (~1470 °C), they could be successfully used at high temperatures [4,5]. The growth of langasite-type crystals, however, need plenty of Ga_2O_3 raw material, which enhance growth price considerably. In order to decrease the cost of crystal growth, people used other elements to replace noble Ga element. In this way, $Ca_3NbGa_3Si_2O_{14}$ (CNGS), $Ca_3TaGa_3Si_2O_{14}$ (CTGS), $Sr_3NbGa_3Si_2O_{14}$ (SNGS) and $Sr_3TaGa_3Si_2O_{14}$ (STGS) were prepared.

Successful single crystal growth of SNGS was first reported by Mill et al. in 1998 [6], and the STGS crystal was reported by B.H.T. Chai et al. in 2000 [7]. There were many reports concerning the structure, piezoelectric, crystal growth and optical properties of SNGS and STGS [8–16]. The band structure and density of states, however, have not been investigated as far as we know. The measurement of the SAW parameters for STGS at Y-cut [17] and SNGS at X, Y, Z cuts [18] shows great promise for SAW applications. But the theory calculation for phase velocity and piezoelectric properties has not been reported.

The first principles method based on density function theory has been proven to be a good and reliable method to reveal the physical properties and microscopic origin of solid materials [19,20]. In this paper, we investigated the optimized geometry structure, band structure and density of states of SNGS and STGS crystals by using the first principles pseudo-potential method, from which the dependence of piezoelectric properties with band structure were discussed. We have also calculated the phase velocity, electromechanical coupling factor and PFA of SNGS and STGS at X, Y, Z cuts by solving Christoffel equation [21]. Compared with the experimental data, we gained better cuts styles of SNGS and STGS, which provide a theoretic basis for their SAW application.

2. Electrical structure calculation

2.1. Calculation method

The density functional theory (DFT) plane-wave pseudopotential method was used to optimize the geometry of the structure

* Corresponding author. Tel.: +86 010 89731990; fax: +86 010 69744849.
E-mail address: luguiwu@sohu.com (G. Lu).

0925-8388/$ – see front matter © 2011 Published by Elsevier B.V.
doi:10.1016/j.jallcom.2011.02.120

and calculate the ground state energy. The generalized gradient approximation (GGA) with the functional proposed by Perdew et al. [22] was employed to evaluate exchange-correlation energy. The Broyden–Fletcher–Goldfarb–Shanno optimization method [23] was used to search for the ground states of crystals. Perdew–Burke–Ernzerhof generalized gradient approximation (PBA-GGA) and pseudopotential were used in optimizing the geometry of the structure, in which the pseudopotential was the ultrasoft pseudopotential [24] of reciprocal space lattice. The energy cut was 350.0 eV, and the SCF convergence tolerance is 1×10^{-6} eV/atom. For the calculation of band structure and density of states, LDA (CA-PZ) and pseudopotential were adopted, in which the pseudopotential was the standard conservation pseudopotential of reciprocal space lattice, energy cut was 500.0 eV, and the SCF convergence tolerance is 2×10^{-6} eV/atom.

2.2. The geometry of the structure

Both SNGS and STGS crystals have a triangular structure, which belong to point group 32, space group *P*321. The lattice parameters were $a = 0.8282$ nm, $c = 0.5073$ nm for SNGS [9] and $a = 0.8293(2)$, $c = 0.5078(2)$ nm for STGS [25]. We have constructed the crystal structure according to the lattice parameters and Wyckoff position for SNGS and STGS, and the optimized structure are shown in Fig. 1.

From the crystal structure of SNGS and STGS, we can find that they are isostructural with CGG [26]. In the case of SNGS and STGS, Sr atoms occupy the decahedral site and Ta and Nb atoms occupy the octahedral site, while the Ga atoms and Si atoms are at the tetrahedral sites. To investigate the ground state of lattice structures of SNGS and STGS, we calculated the lattice parameters, equilibrium volumes and selected interatomic distances. The optimized atomic coordinates are listed in Table 1 and partial lattice parameters and equilibrium volumes are concluded in Table 2. Meanwhile, we listed the atomic coordinates and partial lattice parameters which were obtained by X-ray diffraction in Table 1 and 2. In addition, we calculated the selected interatomic distances of SNGS and STGS which were compared with the experimental values in Table 3. The optimized atomic coordinates and selected interatomic distances

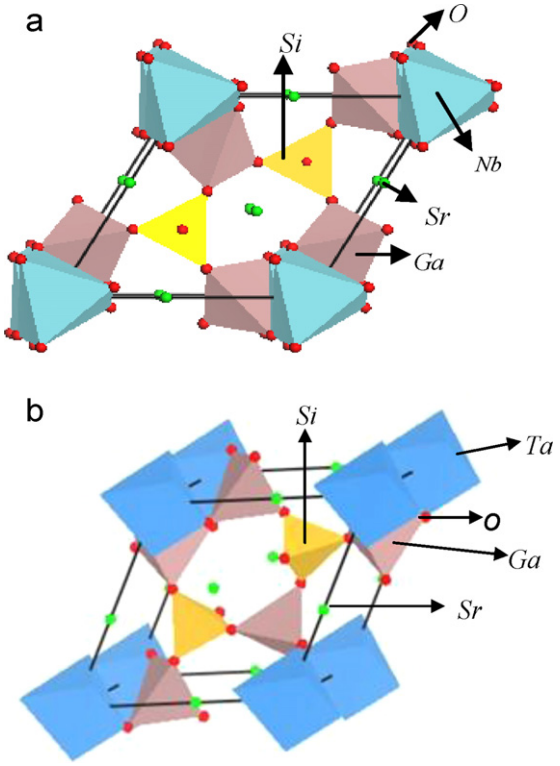

Fig. 1. The unit cell of SNGS (a) and STGS (b).

are in agreement with the experimental results. For the ground state, the calculated equilibrium volume of STGS is litter smaller than the experimental result. It should be noticed that the temperature in the first principle calculation was set to 0 K, while the experimental measurement was measured at room temperature. Thus, we consider that the above discrepancy for the equilibrium volume may be due to the effect of thermal expansion.

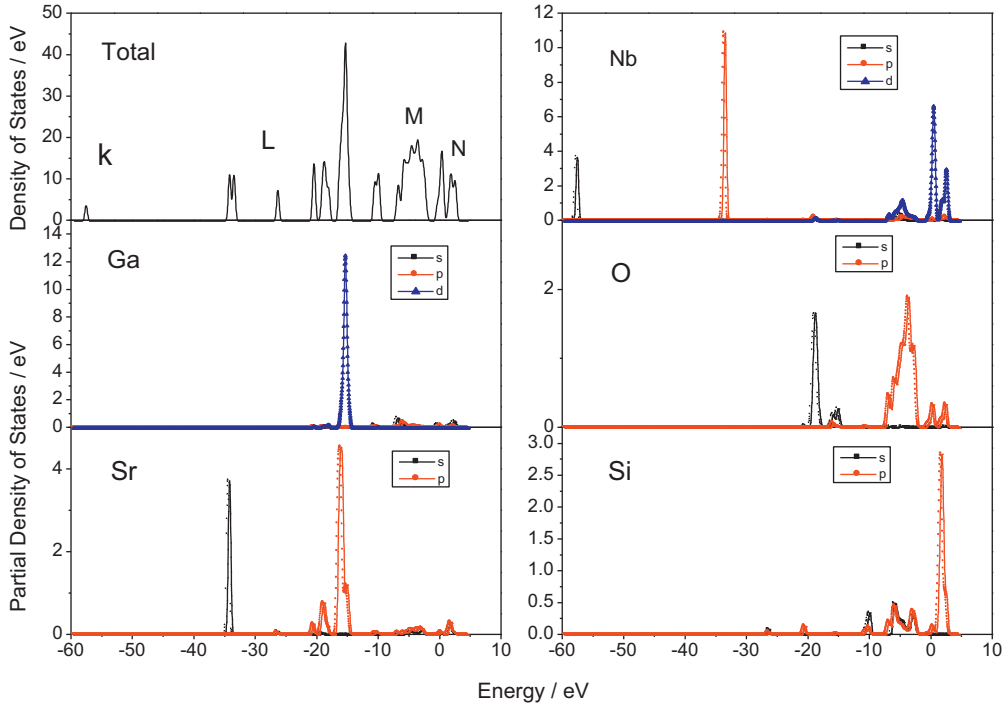

Fig. 2. Density of states and partial density of states of SNGS.

Table 1
The optimized and experimental atomic coordinates.

SNGS	Atom						
	Sr	Nb	Ga	O1	O2	O3	Si
x/a							
Exp	0.42976	0	0.74681	1/3	0.47378	0.24526	1/3
Cal	0.42976	0	0.74681	0.33531	0.47378	0.24526	0.3333
y/b							
Exp	0	0	0	2/3	0.33531	0.05349	2/3
Cal	0	0	0	0.70281	0.3387	0.056	0.6667
z/c							
Exp	0	0	0.5	0.28542	0.70281	0.24021	0.5294
Cal	0	0	0.494443	0.28526	0.70281	0.25021	0.5294
STGS	Atom						
	Sr	Ta	Ga	O1	O2	O3	Si
x/a							
Exp	0.4292(1)	0	0.7464(1)	1/3	0.4742(8)	0.2208(7)	1/3
Cal	0.43368	0	0.744518	0.3333	0.475770	0.232139	0.33333
y/b							
Exp	0	0	0	2/3	0.3067(9)	0.0945(8)	2/3
Cal	0	0	0	0.6667	0.309546	0.0912964	0.66667
z/c							
Exp	0	0	0.5	0.219(2)	0.331(1)	0.7693(9)	0.5341(6)
Cal	0	0	0.5	0.222839	0.32570	0.761507	0.537162

Table 2
Lattice constants and equilibrium volumes.

	SNGS		STGS	
	Cal	Exp	Cal	Exp
a (Å)	8.282	8.282	8.273	8.293(2)
c (Å)	5.073	5.073	5.067	5.078(2)
V (Å^3)	301.3	301.3	300.327	302.462(8)

Table 3
Selected interatomic distances(Å) for (a) SNGS and (b) STGS crystals.

(a)

Sr polyhedron	Cal	Exp	Nb octahedron	Cal	Exp
Sr-O1 × 2	2.54668	2.698(3)	Nb-O3 × 2	1.98021	2.071(6)
Sr-O2 × 2	2.49158	2.496(6)			
Sr-O2′ × 2	2.82858	2.896(6)			
Sr-O3 × 2	2.42699	2.449(6)			
(Sr–O)av	2.57345	2.635			
Si tetrahedron			Ga tetrahedron		
Si-O1 × 2	1.5956	1.614(9)	Ga-O2 × 2	1.84006	1.864(7)
Si-O2 × 2	1.6346	1.712(7)	Ga-O3 × 2	1.8348	1.796(6)
(Si-O)av	1.6151	1.663	(Ga-O)av	1.83743	1.830

(b)

Sr polyhedron	Cal	Exp	Ta octahedron	Cal	Exp
Sr-O1 × 2	2.69801	2.706(3)	Ta-O3 × 2	2.06604	1.976(6)
Sr-O2 × 2	2.49151	2.551(6)			
Sr-O2′ × 2	2.91764	2.913(6)			
Sr-O3 × 2	2.46372	2.516(6)			
(Sr-O)av	2.64272	2.672			
Si tetrahedron			Ga tetrahedron		
Si-O1 × 1	1.59278	1.596(9)	Ga-O2 × 2	1.86695	1.873(7)
Sr-O2 × 3	1.64451	1.648(7)	Ga-O3 × 2	1.83734	1.826(6)
(Si-O)av	1.63158	1.635	(Ga-O)av	1.85214	1.8502

(a) The experience value reference [24].
(b) The experience value reference [23].

Table 4
The elastic constants c_{ij} (10^{-12} Nm^{-2}), piezoelectric constants e_{ij} (Cm^{-1}), relative dielectric constants ε_{ij} and density ρ (g/cm^3) of STGS and SNGS.

	c_{11}	c_{12}	c_{13}	c_{14}	c_{33}	c_{44}	e_{11}	e_{14}	ε_{11}	ε_{33}	ρ
SNGS	160.8	74	82.3	4.5	202.2	55.3	−0.486	0.10	12.4	21.4	4.650
STGS	157.3	69.9	70.4	2.5	188.6	50.8	−0.4204	0.138	17.43	23.73	5.121

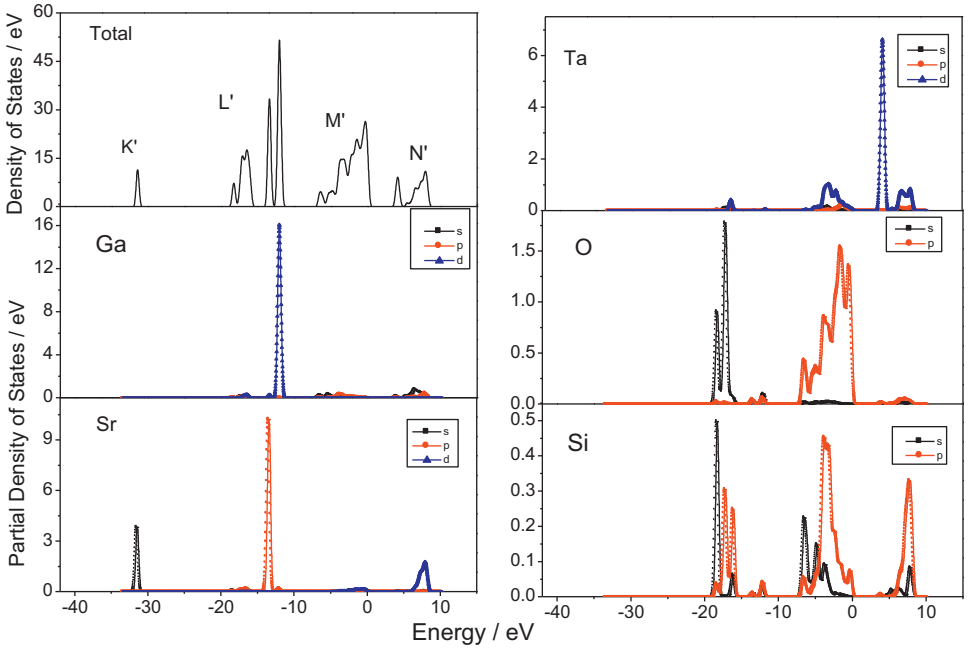

Fig. 3. Density of states and partial density of states of STGS.

2.3. Electrical structure

Figs. 2 and 3 show the calculated density of states (DOS) and partial density of states (PDOS) of SNGS and STGS. It is clear that the PDOS can be divided into four regions. In case of SNGS, the four regions are indicated by K, L, M and N, respectively. The K and L regions belong to low energy band. The K region locates at −58.23 eV and only comes from Nb s orbitals. The L region locates between −35 and −10 eV, where there are five peaks located at −15.44 eV(peak-1), −18.78 eV(peak-2), −20.53 eV(peak-3), −26.44 eV (peak-4) and −33.56 eV(peak-5), respectively. Moreover, the peak-1 as the highest peak mainly consists of Ga d orbitals and Sr p orbitals. The peak-2 is also occupied by Sr p orbitals and the peak-3 and peak-4 are by O s orbitals. The peak-5 mainly comes from Sr s orbitals. Meanwhile, the K and L regions have small contribute to Si s, p orbitals. The M region has a range from −10 to 0 eV as the valence band, in which O p, and Nb d orbitals are included and the nominal composition of Si s, p orbitals are doped. The conduction band is in the N region from 0 eV to 10 eV, which is mainly composed of Nb d and Si p and a few of O p orbitals. We find hybridization between O p orbitals and Nb d orbitals which indicates a certain ionicity characteristic of the Nb–O bonds.

As shown in Fig. 3, the four regions of PDOS of STGS are indicated by K′, L′, M′ and N′, and we can find that the peaks of PDOS of Sr, Ga, Si and O atoms have a tendency of shifting to the higher energy as compared with the PDOS of SNGS. The top of the valence band is due to O p orbitals. The valence band and the conduction band of STGS mainly consist of Ta d orbitals, Sr d orbitals and O p orbitals. Hybridization is also observed between Ta d orbitals and O p orbitals, which indicates the ionicity characteristic of the Ta–O bonds.

In Fig. 4, the band structures of SNGS and STGS are plotted along high-symmetry lines of the first Brillouin zone. In case of STGS, the top of the valence band is at the K-point while the bottom of the conduction band at the G-point. It means that STGS is an indirect-gap material and the indirect band gap is 3.55223 eV. Similar to STGS, SNGS is also an indirect-gap material and the indirect band gap is 0.62117 eV.

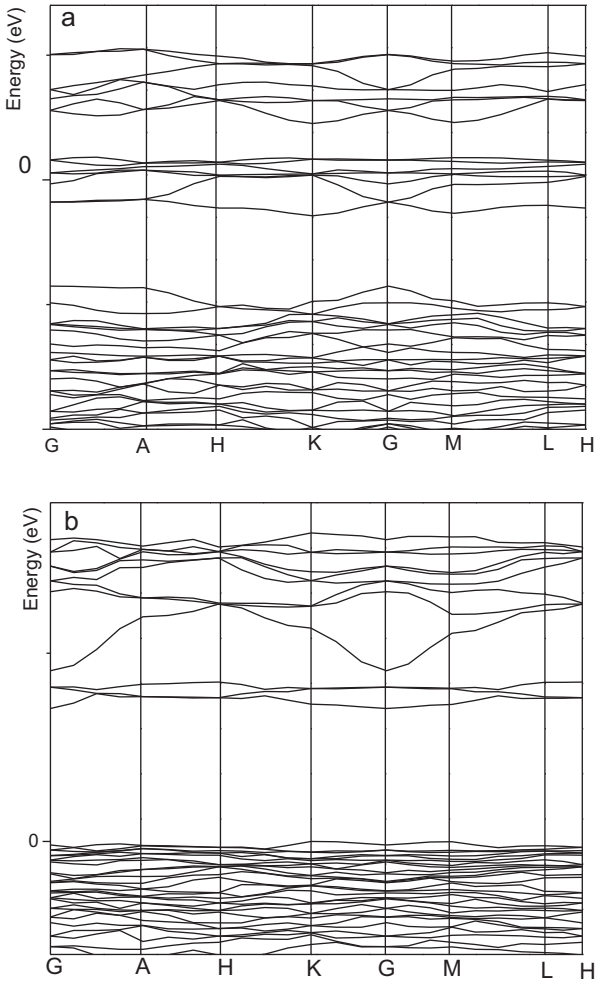

Fig. 4. The band structure of SNGS (a) and STGS (b) along high-symmetry lines of the first Brillouin zone.

3. The SAW properties

3.1. Theory

In order to perform the theoretical calculation, material constants such as elastic, piezoelectric, relative dielectric constants and density are required. The material constants of SNGS and STGS measured separately by Chilla et al. [18] and Yu et al. [27] were used for the present calculation and are given in Table 4.

The cuts types were usually indicated by the Euler angles (φ, θ, χ). Normally, X-cut, Y-cut and Z-cut correspond the Euler angles (90°, 90°, 0°–180°), (0°, 90°, 0°–180°) and (0°–180°, 0°, 0°), respectively. To analyze the SAW properties of any cut type, we should use tensor transformation law to translate the material constants along crystal axis into the cut type along corresponding cut angles.

The elastic (ε), piezoelectric(c), relative dielectric (e) constants along crystal axis is translated into ε', c' and e' along Euler angles (φ,θ, χ) by rigid body rotation and tensor transformation law. The translated relationship can be written as

$$\varepsilon' = (\alpha_1\alpha_2)\varepsilon(\alpha_1\alpha_2)^T, \quad c' = (M_1M_2)c(M_1M_2)^T, \quad e' = (\alpha_1\alpha_2)e(M_1M_2)^T$$

where α_1 and α_2 are third-order tensors and M_1 and M_2 are six-order tensors, and they can be written as

$$\alpha_1 = \begin{bmatrix} \cos\varphi & \sin\varphi & 0 \\ -\sin\varphi & \cos\varphi & 0 \\ 0 & 0 & 1 \end{bmatrix} \qquad \alpha_2 = \begin{bmatrix} 1 & 0 & 0 \\ 0 & \cos\theta & \sin\theta \\ 0 & -\sin\theta & \cos\theta \end{bmatrix}$$

$$M_1 = \begin{bmatrix} \cos^2\varphi & \sin^2\varphi & 0 & 0 & 0 & \sin 2\varphi \\ \sin^2\varphi & \cos^2\varphi & 0 & 0 & 0 & -\sin 2\varphi \\ 0 & 0 & 1 & 0 & 0 & 0 \\ 0 & 0 & 0 & \cos\varphi & -\sin\varphi & 0 \\ 0 & 0 & 0 & \sin\varphi & \cos\varphi & 0 \\ -\frac{\sin 2\varphi}{2} & \frac{\sin 2\varphi}{2} & 0 & 0 & 0 & \cos 2\varphi \end{bmatrix} \qquad M_1 = \begin{bmatrix} 1 & 0 & 0 & 0 & 0 & 0 \\ 0 & \cos^2\theta & \sin^2\theta & \sin 2\theta & 0 & 0 \\ 0 & \sin^2\theta & \cos^2\theta & -\sin 2\theta & 0 & 0 \\ 0 & -\frac{\sin 2\theta}{2} & \frac{\sin 2\theta}{2} & \cos 2\theta & 0 & 0 \\ 0 & 0 & 0 & 0 & \cos\theta & -\sin\theta \\ 0 & 0 & 0 & 0 & \sin\theta & \cos\theta \end{bmatrix}$$

To obtain surface acoustic wave propagation characteristics, we can solve the Christoffel equation with semi-infinite crystal boundary conditions [21]. The coordinate system under investigation is illustrated in Fig. 5. Due to the piezoelectric effect, the equations of elastic and electromagnetic wave must be solved simultaneously for the piezoelectric materials. The two equations

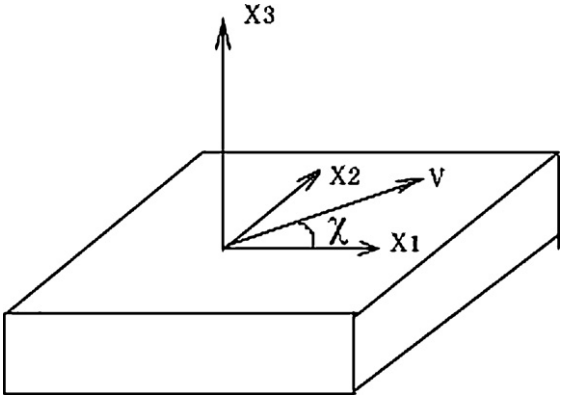

Fig. 5. Coordinate system used in this work.

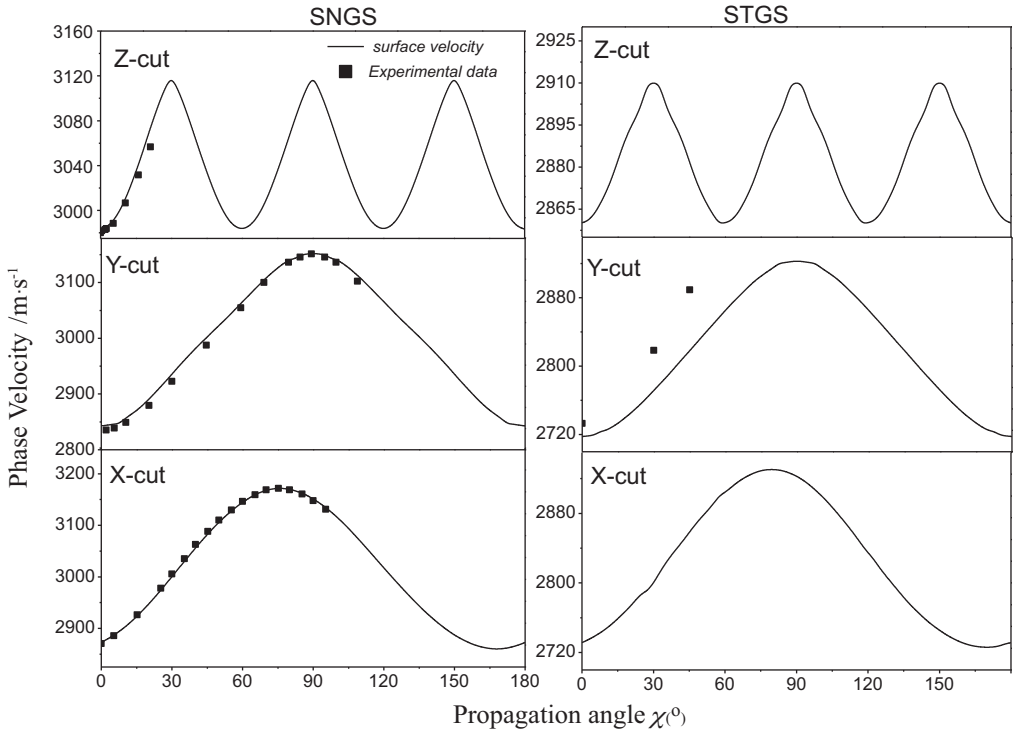

Fig. 6. The free surface phase velocity calculated on SNGS and STGS X, Y, Z cuts and propagation direction (χ).

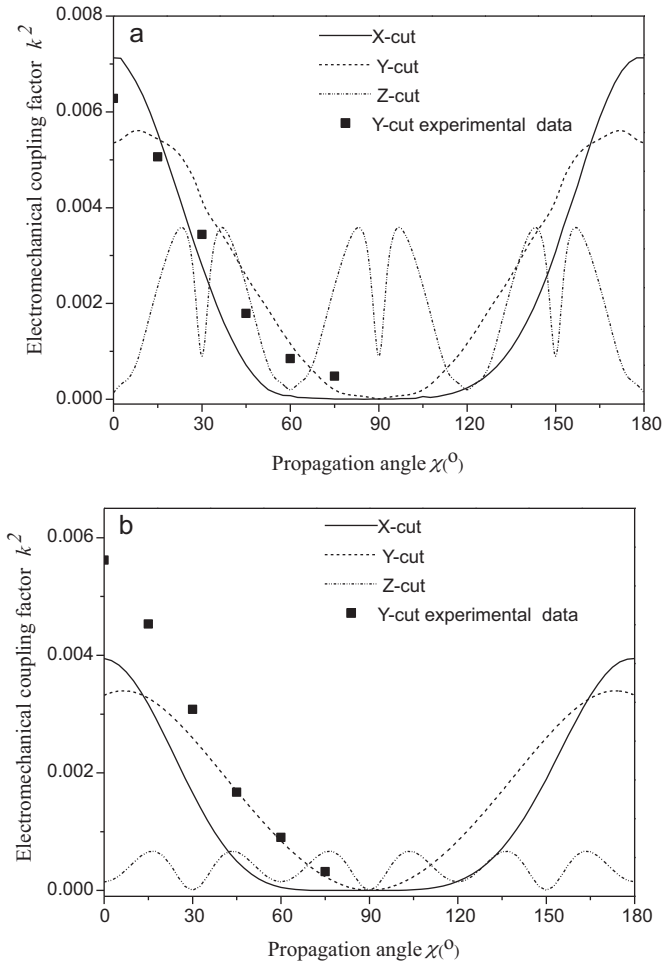

Fig. 7. The electromechanical coupling coefficients calculated on SNGS (a) and STGS (b) X, Y, Z cuts and propagation.

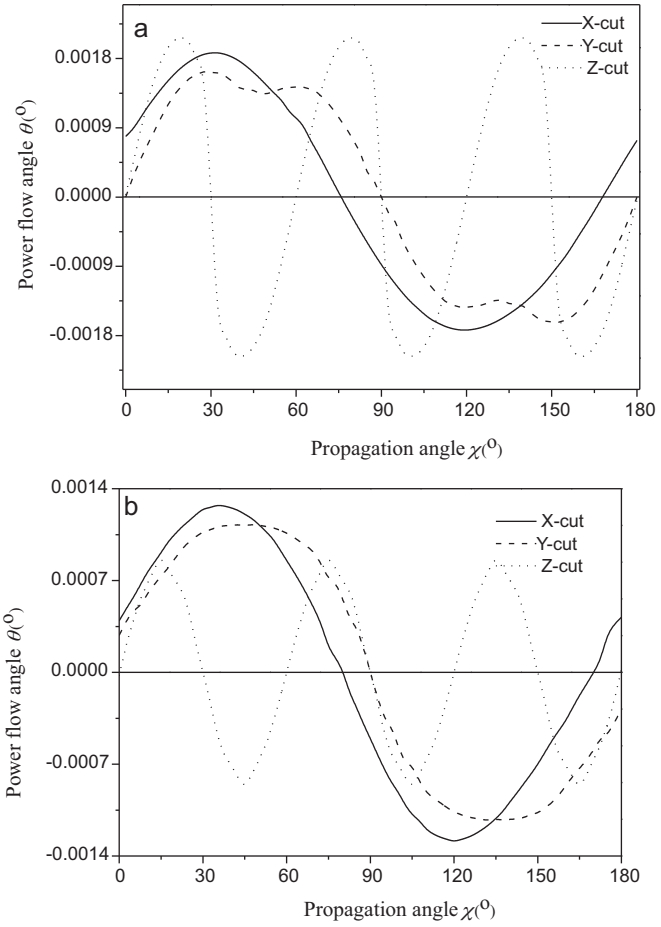

Fig. 8. PFA calculated on SNGS (a) and STGS (b) X, Y, Z cuts and propagation direction (χ).

are coupled by the piezoelectric equations [21]:

$$\begin{cases} c'_{ijkl}u_{k,jl} + e'_{kij}\varphi_{jk} = \rho\ddot{u}_i \\ e'_{jkl}u_{k,jl} + \varepsilon'_{jk}\varphi_{jk} = 0 \end{cases} \quad (1)$$

where u_k is the vibration displacement of the particle, c'_{ijkl} is the elastic stiffness tensor measured under constant electric field, e'_{kij} is the piezoelectric tensor, and ε'_{jk} is the dielectric tensor measured under constant strain, ρ is the density of the medium.

When $\lim_{X_3\to\infty} u = 0$ and $\lim_{X_3\to\infty} \varphi = 0$, the particle displacements and the potential can be written as [21]

$$\begin{cases} u_i = A_i \exp[-jk(vt - l_m x_m)] \\ \varphi = A_4 \exp[-jk(vt - l_m x_m)] \end{cases} \quad (2)$$

$m = 1, 2, 3$where l_m is the direction cosine for the direction of wave propagation, k the scalar of the wave vector, v is the phase velocity of the acoustic wave, and A_i is the amplitude.

Using Eqs. (1) and (2), we can obtain the Christoffel equation [21]

$$\begin{bmatrix} \Gamma_{11} - \rho v^2 & \Gamma_{12} & \Gamma_{13} & \Gamma_{14} \\ \Gamma_{12} & \Gamma_{22} - \rho v^2 & \Gamma_{23} & \Gamma_{24} \\ \Gamma_{13} & \Gamma_{23} & \Gamma_{33} - \rho v^2 & \Gamma_{34} \\ \Gamma_{14} & \Gamma_{24} & \Gamma_{34} & \Gamma_{44} \end{bmatrix} \begin{bmatrix} A_1 \\ A_2 \\ A_3 \\ A_4 \end{bmatrix} = 0 \quad (3)$$

In Eq. (3),

$$\Gamma_{ik} = c'_{ijkl}l_l l_j \quad (i, k = 1, 2, 3), \quad \Gamma_{i4} = e'_{kij}l_k l_j \, (i = 1, 2, 3),$$

$$\Gamma_{ij} = -\varepsilon'_{ik}l_j l_k \, (i = 4, j = 4).$$

The SAW velocities of free and metal surface are v_f and v_m, which can be obtained by solving Eq. (3) in consideration of the boundary conditions of semi-infinite crystal.

Electromechanical coupling coefficient of piezoelectric materials is used to reflect the capacity between energy and power transformation. The strength of the piezoelectric effect can be gauged by the electromechanical coupling coefficient k^2, which is given by the formula [21]

$$k^2 = 2(v_f - v_m)/v_f \quad (4)$$

Power flow angle (PFA) φ is the angle between power flow and phase velocity, which can reflect the diffracted intensity of the sound wave. PFA φ can be given by [21]

$$\tan\varphi = \frac{1}{v}\frac{dv}{d\theta}. \quad (5)$$

4. Results and discussion

Corresponding the propagation angle χ varying from 0° to 180°, free surface phase velocity v_f, electromechanical coupling coefficient k^2 and power flow angle φ are calculated with the X, Y, Z cuts, and the results are shown in Figs. 6–8, respectively. As shown in Fig. 6, the phase velocity varied from 2850 to 3120 m/s for SNGS

Table 5
The SAW characteristics for zero PFA.

Cut types	SNGS			STGS		
	Propagation angle χ (°)	Phase velocity v (m/s)	Electro -mechanical coupling factor k^2 (%)	Propagation angle χ (°)	Phase velocity v (m/s)	Electro-mechanical coupling factor k (%)
	75	3171.68	0.00063	80	2930.6	0
X	167.5	2860.01	0.626	170	2726	0.367
	0	2842.6	0.535	90	2923.1	0
Y	90	3152.4	0			

crystal, from 2720 to 2930 m/s for STGS crystal, respectively. It should be noticed in ones mind that the minimum phase velocity for quartz crystal is 3300 m/s, which means that the SNGS and STGS crystal are of small phase velocity and can be applied in miniaturized devices. Compared with the experiential values [17,18], it can be found that the calculation is in agreement with experimental results. In addition, we can find that the SAW phase velocity of SNGS is much higher than that of STGS.

It is illustrated in Fig. 6 that the curves for the Y and Z-cuts have a central symmetry axis at $\chi = 90°$ and the axis divides the curves into two parts, which are symmetrical to each other. Thus in the later calculation, we can only considered the phase velocities with the corresponding propagation angle from 0° to 90°.

The electromechanical coupling coefficients of SNGS and STGS crystals for the X, Y, Z cuts situations are strongly dependent on wave propagation directions, as shown in Fig. 7. In comparison, the electromechanical coupling coefficients of SNGS and STGS crystals are much higher than that of quartz (less than 0.3%) in most propagation directions. Comparing the electromechanical coupling coefficients of SNGS and STGS crystals for the Y cuts with the experimental data [17], the calculation predicted electromechanical coupling coefficients is basically accurate. In 45°, 60°, 75° of Y-cut STGS cases a good agreement exists between our calculations and the experimental measurements. The difference between calculated and measured 0° of Y-cut SNGS and STGS are much large. Thinking of the litter PFA, the electromechanical coupling coefficients of SNGS and STGS at Z-cut which are all less than 0.1% are not suitable for the further miniaturization of SAW devices. The maximum values of k^2 of SNGS and STGS crystals are 0.712% and 0.4%, respectively, for the X-cut situations.

Fig. 8 shows the calculated φ values for the X, Y, Z cuts cases. Similar to electromechanical coupling coefficients, the PFA value φ is also strongly dependent on the propagation direction. The PFA values of SNGS and STGS crystals are less than 0.00206°, 0.00127°, respectively, as shown in Fig. 8. We also found that cuts of zero PFA of SNGS and STGS which are valuable for making SAW devices.

The SAW characteristics for zero PFA are listed in Table 5. As can be seen from this table, the X-cut SNGS crystal in the direction of propagation direction $\chi = 0°$ gives extremely low phase velocity of 2860.01 m/s and very high electromechanical coupling coefficient of 0.626%, which possess superior SAW performance. In addition, in the propagation direction of 170° of X-cut STGS and 0° of Y-cut STGS are also of excellent piezoelectric characters for making miniatured SAW devices.

5. Conclusion

In summary, the structural, band structure and density of states properties of STGS were investigated using the first-principles method based on the DFT method. In addition, we calculated the phase velocity, electromechanical coupling factor and power flow anger of SNGS and STGS at X, Y, Z cuts. Through calculations, it is found that the temperature has significant effects on the equilibrium volume. The selected interatomic distances are in good agreement with the experimental data. The peaks of partial density of states of Sr, Ga, Si and O of SNGS have a tendency of shifting to the higher energy levels relative to those of STGS. SNGS and STGS are indirect-gap materials and the indirect band gap is 0.62117 eV, 3.55223 eV, respectively. The results show that SNGS and STGS crystals at X-cut and Y cut have excellent SAW properties, such as low phase velocities, small power flow angles and very high electromechanical coupling coefficients, which are all crucial factors for making better SAW devices with broader bandwidth and lower insertion loss. It was found that the phase velocities curves for the Y-cut and Z-cut of SNGS and STGS crystals are symmetric with respect to propagation angle $\chi = 90°$, reflecting the symmetric structure of the SNGS and STGS crystals. The calculated phase velocity of SNGS and STGS are in good agreement with measured results. Considering PFA, phase velocity and electromechanical coupling coefficient, it was concluded that the propagation direction of 167.5° of X-cut SNGS, 0° of Y-cut SNGS and 170° of X-cut STGS possess superior SAW performance.

Acknowledgements

This work was supported by key project of Chinese Ministry of Education (108023) and Scientific Research General Program of Beijing Municipal Commission of Education (KM201010772019).

References

[1] A.A. Kaminskii, B.V. Mill, G.G. Khodzhabagyan, Phys. Status Solidi A. 80 (1983) 387–398.
[2] H. Kawanaka, H. Takeda, K. Shimamura, J. Cryst. Growth 183 (1998) 274–277.
[3] J. Bohm, R.B. Heimann, M. Hengst, J. Cryst. Growth 204 (1999) 128–136.
[4] J. Detaint, J. Schwartzel, A. Zarka, Proc. IEEE Int. Freq. Contr. Symp., 1994, pp. 58–71.
[5] R.C. Smythe, R.C. Helmbold, G.E. Hague, K.A. Snow, IEEE Trans. UFFC 47 (2) 292 (2000) 355–360.
[6] B.V. Mill', E.L. Belokoneva, T. Fukuda, Russ. J. Inorg. Chem. 43 (1998) 1032–1037.
[7] B.H.T. Chai, A.N.P. Bustamante, M.C. Chou, Proc. IEEE Inter. Freq. Control Symp., 2000, pp. 163–168.
[8] Z.M. Wang, D.R. Yuan, Y.S.h. Yin, J. Alloys Compd. 425 (2006) 264–267.
[9] I.H. Jung, A. Yoshikawa, T. Fukuda, K. Ho Auh, J. Alloys Compd. 339 (2002) 149–155.
[10] I.H. Jung, Y.H. Kang, K. Joo, Mater. Lett. 51 (2001) 129–134.
[11] I.H. Jung, A. Yoshikawa, K. Lebbou, T. Fukuda, K.H. Auh, J. Cryst. Growth 226 (2001) 101–106.
[12] Z.M. Wang, D.R. Yuan, X.F. Cheng, J. Cryst. Growth 252 (2003) 236–240.
[13] J.J. Chen, Y.Q. Zheng, Appl. Phys. Lett. 89 (2006) 012901.
[14] R.B. Heimann, M. Hengst, M. Rossberg, Phys. Status Solidi A. 198 (2003) 415–419.
[15] H.F. Qi, A.J. Wei, D.R. Yuan, Mater. Sci. Eng. B 117 (2005) 143–145.
[16] Z.M. Wang, D.R. Yuan, X.Z. Shi, J. Alloys Compd. 373 (2004) 287–290.
[17] D. Puccio, D.C. Malocha, N. Saldanha, IEEE Trans. Ultrason. Ferroelec. Freq. Contr. 54 (2007) 1873–1881.
[18] E. Chilla, R. Kunze, M. Weihnacht, IEEE Ultrasonic Symp. Proc., 2003, pp. 92–95.
[19] C.W. Zhang, Z. Zhang, S.Q. Wang, J. Alloys Compd. 448 (2008) 53–58.
[20] D.X. Li, D.L. Yu, J.L. He, J. Alloys Compd. 481 (2009) 855–857.
[21] B.A. Auld, Acoustic Fields and Waves in Solids, John Wiley & Sons, Inc, New York, 1973.
[22] J.P. Perdew, K. Burke, M. Enzerhof, Phys. Rev. Lett. 17 (1996) 3865–3868.
[23] T.H. Fischer, J. Almlöf, J. Phys. Chem. 96 (1992) 9768–9774.
[24] J.A. White, D.M. Bird, Phys. Rev. B. 50 (1994) 4954–4957.
[25] H. Takeda, J. Sato, T. Kato, K. Kawasaki, Mater. Res. Bull. 35 (2000) 245–252.
[26] B.V. Mill, A.V. Butashin, G.G. Kodzhabagian, Soviet Physics Doklady 27 (1982) 434.
[27] F.P. Yu, D.R. Yuan, S.J. Zhang, J. Phys. D: Appl. Phys. 42 (2009) 085112.